Stacking faults in homoepitaxy on Ir(111): Detection, evolution with film thickness, and associated defect patterns

Sebastian Bleikamp,[1,2,*] Arne Thoma,[2,†] Celia Polop,[2,‡] and Thomas Michely[1]
[1]*II. Physikalisches Institut, Universität zu Köln, 50937 Köln, Germany*
[2]*I. Physikalisches Institut, RWTH Aachen, 52056 Aachen, Germany*
(Received 10 April 2008; published 18 June 2008)

Scanning tunneling microscopy and low energy electron diffraction are used to investigate the evolution of the stacking fault covered surface area during growth and annealing of thin Ir films on Ir(111). Key elements driving the evolution of faulted surface area with film thickness are identified.

DOI: 10.1103/PhysRevB.77.245424 PACS number(s): 61.72.Nn, 61.72.Mm, 68.55.A−, 61.05.jh

I. INTRODUCTION

Stacking faults are among the most abundant defect structures in thin films and nanostructures. Formation of stacking faults requires only little energy (the stacking fault energy) and due to their low energy, kinetically they are hard to avoid in growth processes, which usually take place far from thermodynamic equilibrium.

Although stacking faults may cause desirable effects, e.g., remnant magnetization in small Pd nanocrystals,[1–4] more commonly they cause a deterioration of properties. Stacking faults and the ensuing formation of twin crystallites are known to critically influence and deteriorate the properties and functionality of films and devices. For example, twin boundaries give rise to quantum well states in SiC (Ref. 5) and cause degradation of the active area in devices through fault expansion under operation conditions.[6] In metal nanowires, scattering at twin boundaries is of especial importance for the electronic properties due to the fact that the lateral dimensions become comparable to the electron mean-free path.[7] In ultrathin epitaxial layers of magnetic materials the stacking sequence is decisive for the magnetic properties.[8]

Thus it is of crucial importance to limit the number of stacking faults and strategies for their avoidance are needed. A prerequisite for such strategies is a thorough understanding of the kinetics of stacking fault formation, propagation, and associated defect structures. Recently, a number of experimental and theoretical studies investigated the behavior of stacking faults in well defined systems and down to the atomic scale.[8–13] Here we report on our studies of the evolution of stacking fault associated defect structures in thin Ir films on Ir(111) with film thickness and annealing temperature. Our manuscript extends to previous studies on the atomic scale mechanisms of stacking fault proliferation in thin Ir films with increasing film thickness.[14] After an overview on growth morphology in homoepitaxy on Ir(111) at 350 K we will describe in detail scanning tunneling microscopy (STM) and low energy electron diffraction (LEED) methods to quantify the fraction of faulted or twinned surface area. The surprising thermal stability of stacking faults in thin Ir films allows to test STM and LEED methods of fault area detection against each other. We identify the defect structures related to stacking faults which laterally separate faulted and unfaulted areas or areas with faults in different layers. They decisively influence surface morphology and cause a transition from layer-by-layer to a rough defect dominated growth mode. For simple situations the atomic arrangement of atoms in these defect structures is discussed. Finally, we demonstrate an enhanced fault island nucleation in the presence of steps, an effect which strongly influences the initial stages of thin-film growth.

II. EXPERIMENT

The experiments were performed in an ultrahigh vacuum (UHV) chamber with a base pressure $P<5\times10^{-11}$ mbar. The sample was cleaned by repeated cycles of sputtering at 1100 K with a mass selected 1 keV Xe^+ ion beam and annealing at 1600 K. Prior to deposition the sample was flashed to a temperature ensuring desorption of all species that might have adsorbed from the background gas. Ir was evaporated from a current heated Ir wire with a standard deposition rate of 1.3×10^{-2} ML/s, where 1 ML (monolayer) is the surface atomic density of the Ir(111) surface. Special care has been taken to ensure clean deposition conditions ($P<1\times10^{-10}$ mbar). Precise calibration of the deposited amount Θ was achieved through coverage determination with STM after fixed deposition time intervals. Imaging was performed with a magnetically stabilized beetle STM.[15] The topographs displayed are differentiated images which appear as if illuminated from the left. On differentiated topographs of rough surfaces features in all layers possess an increased visibility. The STM topographs are post processed with the WSXM software.[16] LEED images and I/V characteristics were measured using a standard three grid rear view LEED optics.

III. MORPHOLOGICAL EVOLUTION AT 350 K

Figure 1 shows snapshots of the surface morphological evolution up to 5 ML deposited. From the images an initial layer-by-layer growth of Ir on Ir(111) is obvious. Even after 5 ML deposited [compare Fig. 1(f)] the fifth layer is almost perfectly closed with only small areas of grooves and islands and a very small area fraction (a few 10^{-3}) on top of islands. Although the neighboring 6*d* transition metals, Ir and Pt are quite similar in their chemical properties, the observed Ir growth behavior on Ir(111) is in marked difference to the one of Pt on Pt(111). At the same temperature—scaled with respect to the corresponding cohesive energy—Pt on Pt(111) displays the growth of mesa mounds separated by grooves of several layer depth.[17] Generally, for 5 ML deposited and

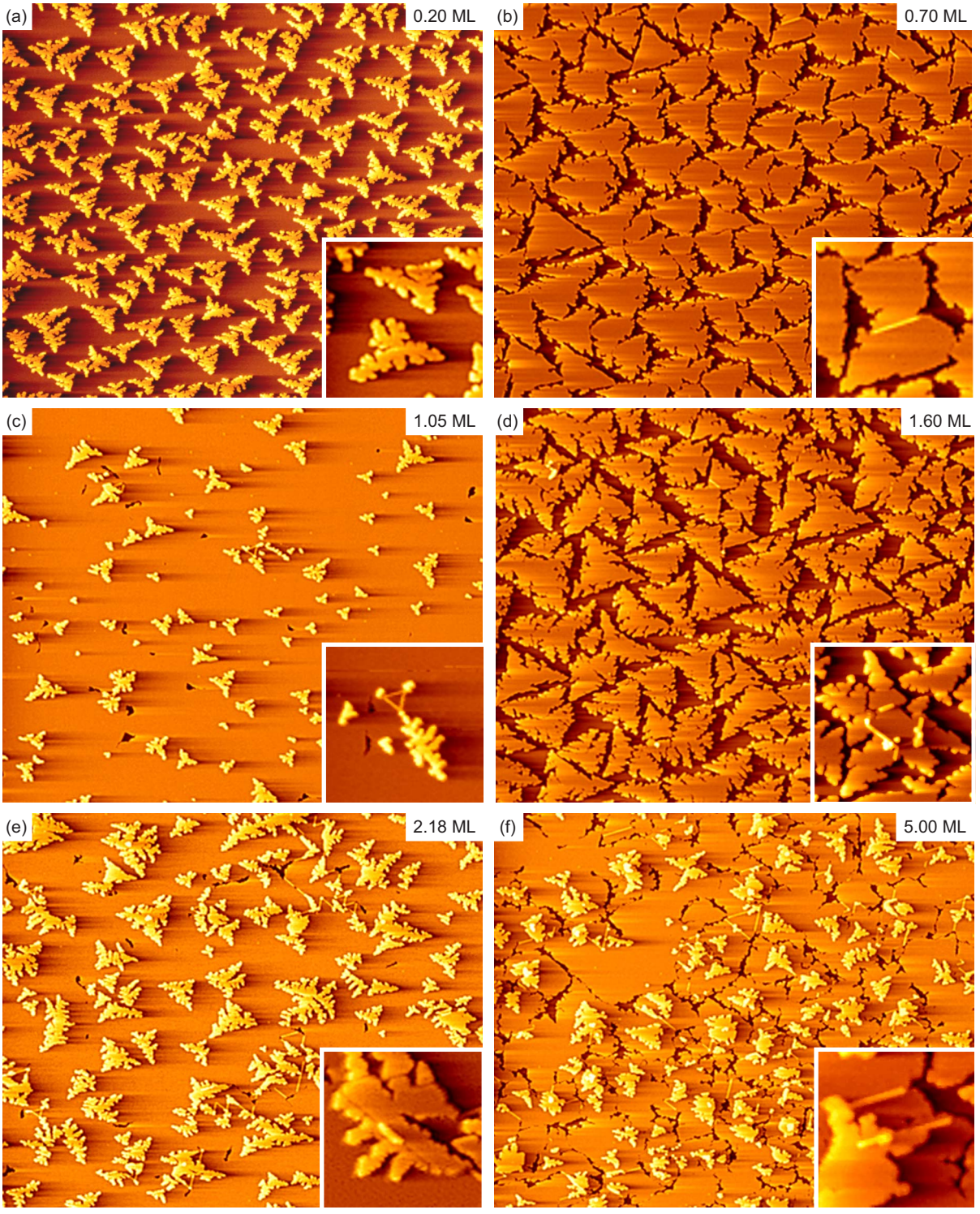

FIG. 1. (Color online) STM topographs after deposition of (a) 0.20 ML, (b) 0.70 ML, (c) 1.05 ML, (d) 1.60 ML, (e) 2.18 ML, and (f) 5.00 ML of Ir on Ir(111) at 350 K. The image size is always 240 nm $\times$ 198 nm. Insets: Characteristic morphological features and defects in magnified view. See text.

temperatures up to 650 K the roughness for the same scaled temperature is always significantly lower on Ir(111) compared to Pt(111).[18] While for Pt homoepitaxy on Pt(111) a significant though temperature dependent-effective step edge barrier is operative;[17] this is not the case for Ir(111). In contrast, once Ir adatoms reach a descending step, they are trapped, unable to return to the terrace and eventually descent.[19] Thus, while the step edge barrier on Pt(111) enhances the nucleation probability on top of islands and thereby makes growth rough, the efficient incorporation of adatoms into descending steps on Ir(111) keeps the surface smooth.

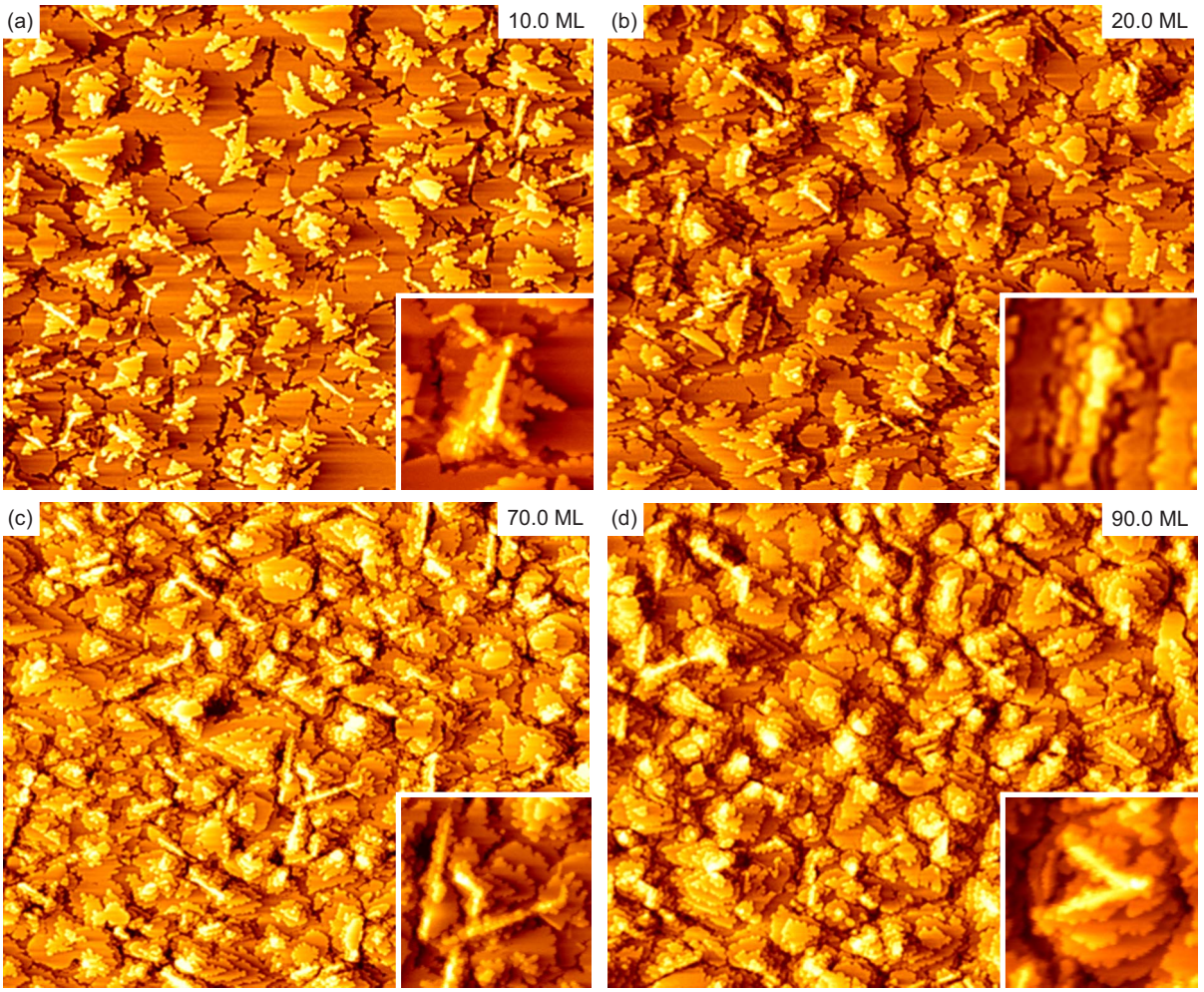

FIG. 2. (Color online) STM topographs after deposition of (a) 10 ML, (b) 20 ML, (c) 70 ML, and (d) 90 ML of Ir on Ir(111) at 350 K. Image size is 240 nm × 198 nm. Insets: Characteristic morphological features and defects in magnified view. See text.

Shortly after nucleation the adatom islands display threefold symmetric fractal-dendritic island shapes [compare Figs. 1(a), 1(c), 1(e), and 1(f)], which become fatter and more compact when the islands approach coalescence [compare Figs. 1(b) and 1(d)]. The dendritic island shapes can be well reproduced by kinetic Monte-Carlo simulations using atomistic input parameters based on field ion microscopy measurements.[20] The more compact island shapes prior to coalescence are due to enhanced supply of atoms descending from the islands filling preferentially the island fjords.

For all topographs in Fig. 1, not one, but two different roughly threefold symmetric island shapes are visible, which are rotated by 180° with respect to each other [compare inset of Fig. 1(a)]. The majority islands with one triangle tip pointing downwards are regular islands while the minority species with one triangle tip pointing upwards are stacking faults islands, as discussed below.

The insets of Figs. 1(b)–1(f) all highlight characteristic defect structures in the film. These are lines of atoms oriented along the dense-packed ⟨110⟩ directions, which are for the smaller deposited amounts [Figs. 1(b) and 1(c)] only one atom wide (named thin decoration rows[14]) but become occasionally also two or more atoms wide (named fat decoration rows[14]) for larger deposited amounts [compare Figs. 1(c)–1(f)]. These decoration rows separate areas of different stacking sequence. The decoration rows tend to start or end in grooves, indicating that phase boundaries of differently stacked areas are frequently hidden in these grooves.

Figure 2 shows snapshots of the surface morphological evolution for $\Theta = 10$ ML up to $\Theta = 90$ ML. Apparently for these thicker films the layer-by-layer growth is lost. The morphology becomes rather heterogeneous. It is dominated by mounds, which are frequently elongated along one of the ⟨110⟩ directions and are of needlelike shape. Also deep grooves are apparent. The insets highlight that these structures are essentially wide decorations rows, from which materials starts to grow partly away. The association of mounds with decoration rows suggests that decoration rows are places of preferred heterogeneous nucleation, giving rise to the onset of three-dimensional mound formation. In a previous publication we reported that the characteristic lateral length scale in this stage of growth is set by the concentration of decoration rows.[14] Based on the visual impression given by the STM topographs one would state a growth mode transition from layer-by-layer growth to a heterogeneous mound growth for Θ somewhere around 10 ML. The

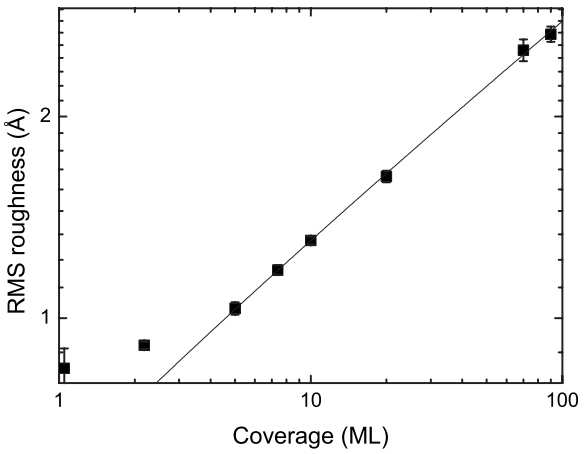

FIG. 3. RMS roughness for coverages up to 90 ML. The line represents a fit to a power law with an exponent $\beta=(0.31\pm0.01)$.

quantitative roughness evaluation shown in Fig. 3 suggests this transition to take place already at 5 ML. It displays a power law for the increase of roughness with coverage for deposited amounts $\geq$5 ML with a growth exponent $\beta=(0.31\pm0.01)$. Only for smaller Θ the roughness shows a slower increase.

As suggested by our description, the key for understanding the unusual growth behavior of Ir on Ir(111) is the decoration rows of various types, which are intimately linked with the presence of stacking faults in the thin film. To this end, prior to a more detailed discussion we present methods suitable for the determination of the faulted surface area.

IV. STACKING FAULT DETECTION

In order to characterize the evolution of stacking faults and their influence on the thin-film morphological evolution, we use the fraction of surface area in faulted stacking θ_F. The meaning of θ_F and how it is measured will be come evident in this section.

A. Direct observation of stacking faults in the first monolayer by scanning tunneling microscopy

As already pointed out and visualized in the inset of Fig. 1(a), islands in the first monolayer point in two opposing directions rotated by 180°. The reason for the two triangle orientations is as follows: Due to the potential-energy landscape at the step edge, Ir islands on Ir(111) are predominantly bounded by {111} microfacetted steps[20] (*B* steps) along the ⟨110⟩ directions. As visualized in Fig. 4 the preference for *B* steps implies immediately the apparent 180° rotation of faulted islands. For a given Θ prior to island coalescence, faulted and regular islands have the same average island size. Determining the nucleation probability P_F for a stacking fault island—the fraction of faulted islands—yields the surface area in faulted stacking as $\theta_F=P_F\Theta$. The stacking fault probability for nucleation on the substrate layer is simply obtained by evaluating the fraction of islands in fault island orientation (apparent rotation by 180°). On the

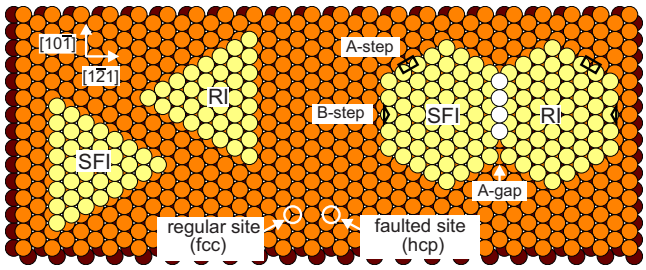

FIG. 4. (Color online) Ball model of the Ir(111) with triangular islands bounded by {111} microfacetted or *B* steps in regular (RI) and a faulted (SFI) stacking sequence (see text). Also shown are a faulted and a regular hexagonal island in close encounter, forming a narrow gap consisting of two {100} microfacetted steps (*A* steps) which form an *A* gap of fourfold coordinated adsorption sites. The *A* gap is decorated by a monatomic chain of atoms oriented along ⟨110⟩. Regular and faulted triangular adsorption sites are also indicated.

substrate layer, layer zero is $P_{F,0}=11\%$ for 350 K (compare Ref. 21).

When islands coalesce, an efficient self-healing effect mechanism as described in detail in Ref. 22 sets in which largely transforms faulted islands to regular stacking. This process takes place when a regular and faulted island have approached such that they are only separated by a gap of subatomic width formed by two *B* steps (compare Fig. 4). Then through atomic jumps of atoms over the gap at kink positions within *B* gaps from a faulted to a regular position, the size of the faulted area decreases. This process comes to a rest, if the sticky *A* gap displaying fourfold coordinated adsorption sites becomes decorated by atoms. Thus, in a partly coalesced island with a fault island envelope, the position of a decoration row marks the part of the island that has been transformed already to regular stacking, as visible in the inset of Fig. 1(b).

B. Stacking faults detection after deposition of a few monolayers by scanning tunneling microscopy

After completion of the first layer the self-healing mechanism leaves only small patches in faulted stacking sequence. Such patches are bounded by decoration rows. Partly, the boundary of such patches may also consist of grooves reaching down to the substrate layer. Taking into account these patches and the amount of faulted area due to fault islands on the upmost connected layer yields again θ_F.

For island nucleation in subsequent layers we surprisingly find a clear increase of P_F. Taking into account only islands not attached to decoration row structures, $P_{F,1}=33\%$ for nucleation on the first deposited monolayer and $P_{F,2}=41\%$ for nucleation on the second deposited monolayer. Both values are much larger than $P_{F,0}=11\%$ obtained for nucleation on the substrate layer. The increased P_F in higher layers must be assumed to cause an increase of in the maxima of θ_F prior to the onset of self-healing by island coalescence. Indeed, the maximum value for θ_F increases from $\theta_F=7\%$ for $\Theta=0.7$ ML to $\theta_F=21\%$ for $\Theta=1.6$ ML. It will be shown below that steps play a crucial role for this increase.

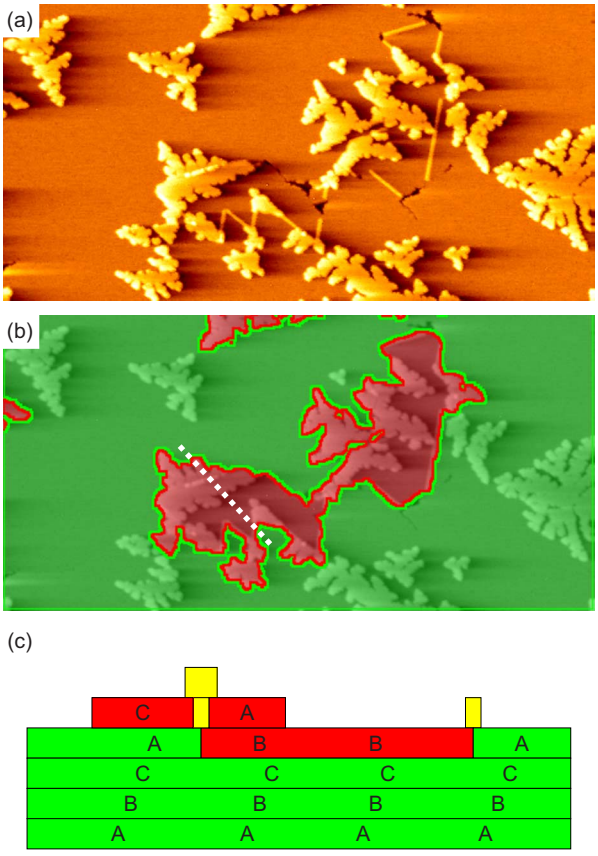

FIG. 5. (Color online) (a) STM topograph after deposition of 2.18 ML at 350 K. (b) STM topograph as in (a) but with faulted areas dark gray (color online: red) and unfaulted areas shaded light gray (color online: green). (c) Schematic intersection of the crystal along the dotted white line in (b) indicating the stacking sequence.

An example for the determination of θ_F is shown in Fig. 5 after deposition of 2.18 ML. Figure 5(a) displays an area with a large number of decoration rows and islands attached to them. The associated fault island area is identified in Fig. 5(b) and shaded dark gray (color online: red). The faulted area is bounded by decoration rows, grooves, and islands in the top layer. The islands in the top layer in this area possess all the characteristic fault island orientation. The interpretation is as follows: At the location of the islands initially only decoration rows were present. Attachment of additional atoms to the decoration rows results in island growth. As described in our previous publication on stacking fault influenced growth,[14] stacking faults in two subsequent layers (intrinsic stacking faults) are energetically avoided (see also below). Thus, the material is attached in such a way that the adatom islands growing toward the inside of the area with the fault located in the first layer does not introduce an additional fault in the second layer. Based on a ball model analysis this implies that the islands growing toward the outside are in fact fault islands. Thereby the faulted area increases and fault proliferation takes place.[14] One of the larger second layer islands carries already again a decoration row, but of two atom width. The schematic sketch of the layer stacking along the dotted black line in Fig. 5(c) clarifies the stacking sequence. It should be mentioned that the two atom wide decoration row (a fat decoration row) now separates two faulted areas with faults in different levels rather than a faulted and a regular area as for the thin one atom wide decoration rows. As will be discussed below, in general a fat decoration row separates two faulted areas with faults in different layers and the width of the decoration row increases with the depth of the faults.

Here is also the place for a remark on terminology. For stacking fault areas thicker than one atomic layer it is more common to talk of twin crystallites. The substrate layer, a faulted layer, and a third layer on top, not introducing a new fault with respect to fcc stacking, is a three layer system defining again a fcc-stacking sequence. This sequence defines a twin crystallite, which becomes indistinguishable from the original crystal in symmetry if rotated by 180° through an axis normal to the plane of the stacking fault. This implies that an additional stacking fault several layers above the initial one will cancel its effect and a buried twin crystallite results. In top view the surface area will appear free of faults. However, once fat decoration rows are formed, they pin the stacking sequence in their neighborhood and fault cancellation does not take place.[14] The plane of the stacking fault is usually termed coherent twin boundary.[23] It is the grain boundary with the lowest energy, about 0.09 eV per atom for Ir,[21,24,25] and displays no change of atom coordination (and thus density) or distance over the boundary. The boundary laterally separating grains twinned in different layers or twinned grains from untwinned ones is named incoherent twin boundary.[23] For the case of Ir(111) the incoherent twin boundaries are boundaries of reduced density, giving rise to the observable decoration row structures (see also below).

C. Measuring the surface area of twin crystallites by low energy electron diffraction

With increasing Θ the STM method for determination of θ_F becomes more and more ambiguous, and for $\Theta > 5$ ML the method is not more applicable.

If we consider the surface to be formed by regular and twin crystallites, defined in each case by three properly stacked layers, LEED appears to be the ideal method for the determination of θ_F. LEED is surface sensitive and the diffracted intensity results to a very good approximation from the topmost three layers. Thus for an entirely twinned crystal of at least three layer thickness the intensity I versus electron energy E, curves (I/V curves) are identical to those of an untwinned crystal, but with the I/V curves of the (10) and (01), diffraction spots interchanged. With $I_{10}(0,E)$ and $I_{01}(0,E)$ being the I/V curves of the (10) and (01) spots of the clean surface, respectively, the intensity $I_{10}(\Theta,E)$ of a (10) spot of a partly twinned surface may be expressed as follows:

$$I_{10}(\Theta,E) = (1-\theta_F)I_{10}(0,E) + \theta_F I_{01}(0,E). \quad (1)$$

The method described relies on the assumption of a surface composed of twin crystallites and regular crystallites, i.e., on the assumption that the stacking faults are two or more layers underneath the surface. While this assumption is

evidently not fulfilled for only a few monolayers deposited, in the regime where the surface morphological evolution is dominated by heterogeneous nucleation at the defect structures, i.e., for $\Theta > 10$ ML, it is fulfilled to a good approximation. As then homogeneous nucleation is largely absent, no new faults are introduced in the top layer. The change of θ_F is then largely due to the lateral shifts of boundaries between regular and twin crystallites and is a slowly varying function of Θ

Figure 6 displays an example for the application of this method. For a 90 ML thick film grown at 350 K, both $I_{10}(90\ \mathrm{ML}, E)$ and $I_{01}(90\ \mathrm{ML}, E)$ are fitted with the single parameter θ_F on the basis of our measured $I_{10}(0, E)$ and $I_{01}(0, E)$. As visible in Figs. 6(b) and 6(c) the measured and fitted spectra coincide with high perfection with a Pendry R factor of 0.12.[26,27] We note that slightly annealed films show unchanged θ_F but a considerably reduced Pendry R factor (e.g., $R=0.07$ after annealing to 850 K), most likely due to reorganization of the atoms in extended defect structures to lattice positions, either of regular or faulted crystallites (see below).

D. Twin crystallite identification in annealed films by scanning tunneling microscopy through post decoration

The high stability of the twin crystallites formed during Ir homoepitaxy against thermal healing offers a unique possibility to apply a post decoration method previously used in TEM studies of epitaxial growth.[28] The method requires sufficiently large terraces, such that homogeneous nucleation of new islands upon Ir deposition takes place. During annealing to 850 K surface diffusion is efficient enough to smoothen the surface to an extent such that upon room-temperature deposition new Ir islands nucleate on the terraces formed. While in regular areas the triangular envelope of the newly formed islands will point downward with a probability of about 90%, in the faulted areas they will point upward with the same probability. The differing predominant orientations of the islands together with the finding that twinned and untwinned areas are separated by steps (not necessarily of monatomic height) allows straightforward determination of θ_F.

Figure 7 displays an example for the application of the post decoration method after annealing a 90 ML film to 1200 K.

E. Quantitative comparison of low energy electron diffraction and scanning tunneling microscopy methods applied to annealed films

For smooth annealed films the results for θ_F obtained by the STM post decoration method and from fitting LEED I/V curves may be compared to each other. The comparison is exemplified in Fig. 8 for an annealing sequence of a 90 ML thick film grown at 350 K. According to the LEED measurements $\theta_F \approx 0.6-0.65$ up to 1050 K; after annealing to 1200 K it is still above 0.5, and does not vanish at all after annealing to 1350 K, the highest temperature applied in this sequence. The interesting details of the real-space structure of the annealed thin films and the origin of the remarkable stability of the twinned films are not within the scope of the present manuscript and will be addressed in a separate publication.[29] For the films annealed to 850 K and higher temperatures the STM post decoration method could be applied. The results agree within the limits of error with the LEED I/V curve method. The larger error margins of the STM post decoration method after annealing to high temperatures are caused by the large domain sizes. As the STM topographs are limited in size, the large domains cause significant fluctuations in θ_F.

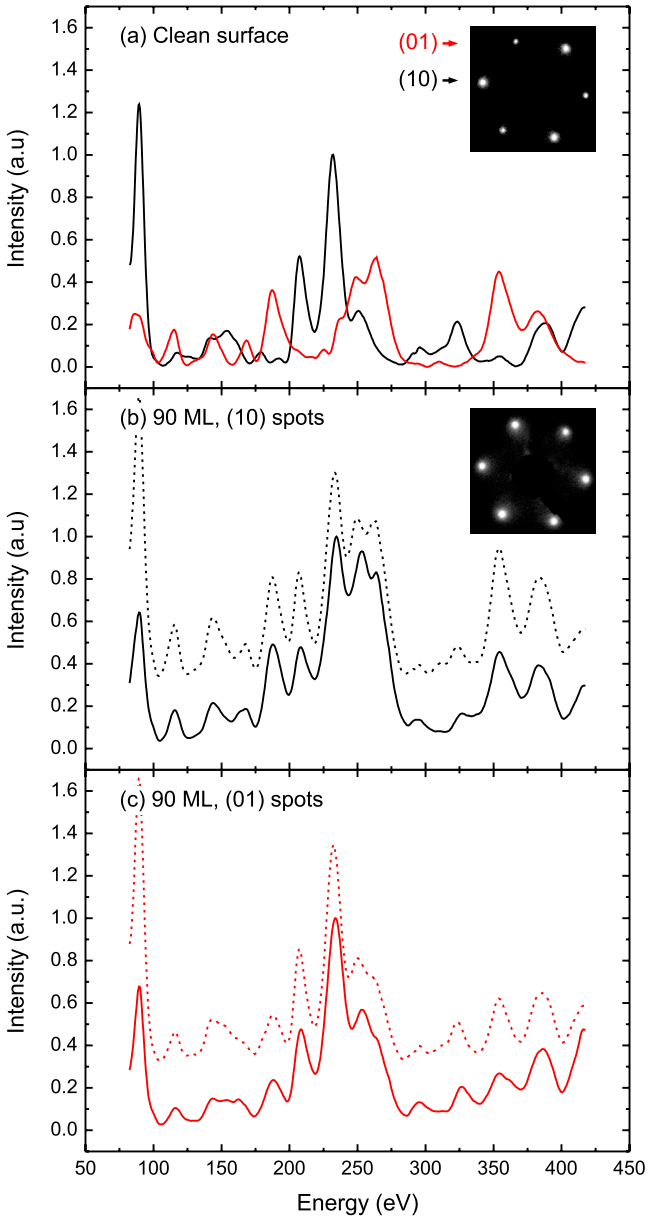

FIG. 6. (Color online) (a) LEED intensity I versus electron energy E curves $I_{01}(0, E)$ and $I_{10}(0, E)$ of the clean surface (0 ML deposited) for the (10) (black) and (01) (red) spots, respectively. (b) Measured (full line) and fitted (dotted line) intensity $I_{10}(90\ \mathrm{ML}, E)$ after deposition of 90 ML at 350 K. (c) Measured (full line) and fitted (dotted line) intensity $I_{01}(90\ \mathrm{ML}, E)$ after deposition of 90 ML at 350 K. In (b) and (c) measured and calculated curves are offset with respect to each other for clarity. Insets: LEED images at 235 eV.

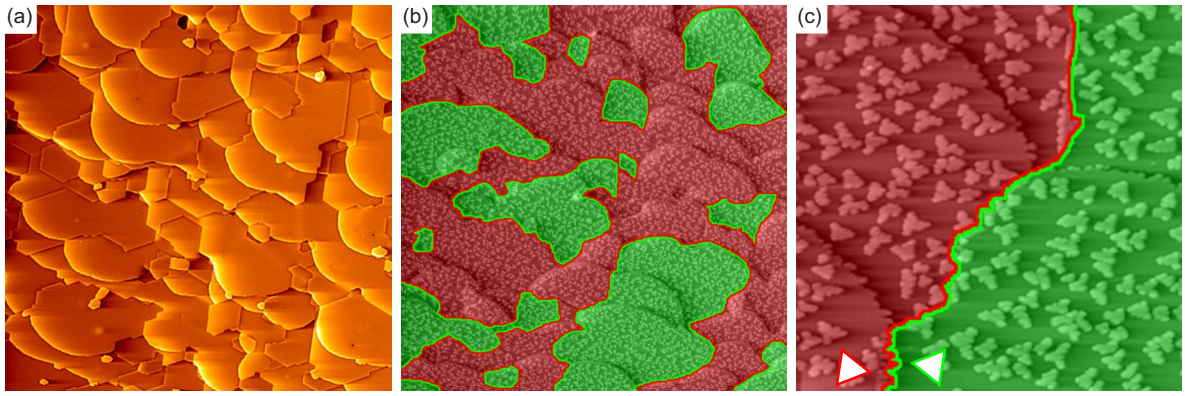

FIG. 7. (Color online) Illustration of the post decoration method for the detection of twinned surface areas. (a) Surface after deposition of 90 ML at 350 K and additional annealing to 1200 K for 180 s. (b) and (c) Surface after decoration through approximately 0.2 ML Ir at room temperature. Twinned areas are shaded dark gray (color online: red), untwinned areas are shaded light gray (color online: green). The areas are identified by the predominant orientation of the triangular envelope of the decorating islands indicated in (c) through white triangles. Image sizes: 500×500 nm for (a) and (b) and 105×105 nm for (c).

We compared the LEED I/V curve and the STM post decoration methods for annealing sequences of several films and always found the values for θ_F to agree better than 10%. However, there is a clear tendency for the STM post decoration method to yield slightly larger values for θ_F which is also visible in Fig. 8. The origin of this difference is traced back to the different surface area sampling by LEED and STM. For the STM analysis largescale topographs are needed. Such topographs are usually taken in relatively smooth surface areas with a limited number of pre-existing steps. In regions where the initial step distribution formed step bundles (such regions always exist) largescale topographs are hardly taken due to the large height variations which make imaging difficult. In such regions with small initial terrace sizes, step flow growth is prevalent even at 350 K. Due to the growth away from steps in regular stacking sequence, twin crystallite formation is absent or at least rare. While STM sampling excludes such areas, LEED as a macroscopically averaging method includes the intensity contribution from the step bundle areas and thus obtains a smaller value for θ_F.

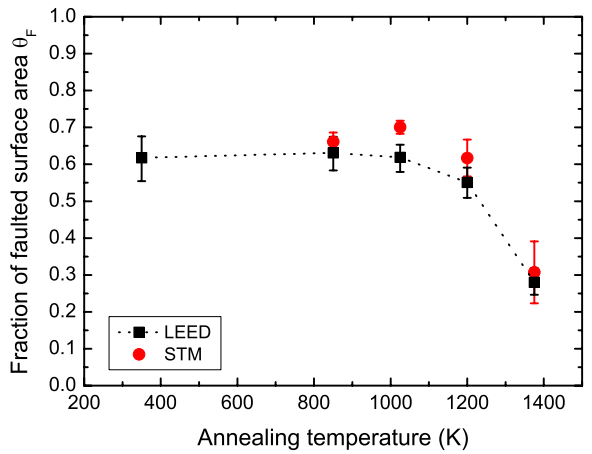

FIG. 8. (Color online) Comparison of θ_F for a 90 ML Ir film measured by LEED (full black squares) and STM (full red circles) after subsequent annealing steps of 180 s to the temperatures indicated. Lines are guides to the eye.

V. DISCUSSION

A summary of the measurements for θ_F with the different methods discussed in the Sec. IV is shown in Fig. 9. Different amounts of Iridium were deposited at 350 K without subsequent annealing. The quantity θ_F shows in the range of a few layers clear oscillations and then increases to values considerably larger than 50%. This behavior is inconsistent with any simple model assuming a fixed and layer independent probability to introduce a stacking fault. Such a model would approach a limiting value $\theta_F = 0.5$.

In the initial phase of growth the fraction of surface area in faulted stacking θ_F is oscillatory with monolayer period. The first two oscillations for θ_F are visible in Fig. 9. Based on the fact that layer-by-layer growth is still present at 5 ML, it is likely that the oscillations continue at least up to 5 ML deposited. This reasonable speculation is indicated by the dotted line in Fig. 9. Note that the full straight lines in Fig. 9 just connect the data points. The origin of the oscillations is the self-healing mechanism already mentioned above which

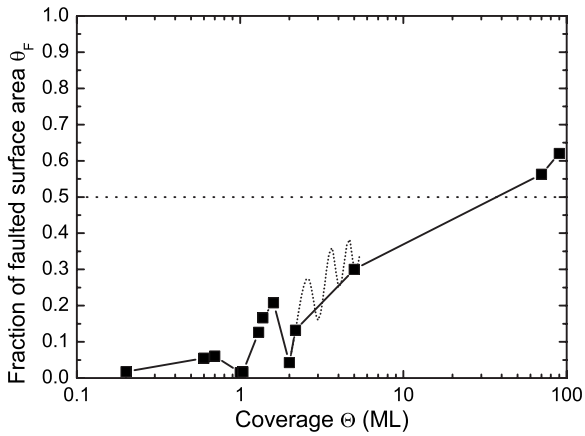

FIG. 9. Fraction of surface area covered by stacking faults θ_F versus Θ. Full black squares: Experimental data, lines to guide the eye. Dotted line: Probable behavior of θ_F between experimental data points. Data below $\Theta = 10$ ML measured by STM and above by LEED. All films grown at 350 K without annealing.

removes, in a growing layer, most of the newly formed stacking fault upon layer closure. The value of θ_F in the oscillation minima is increasing with Θ. Note that if the oscillations persist up to 5 ML, the data point at $\Theta=5$ ML is a minimum value, since Fig. 1(f) displays a situation at layer closure. The amplitude of the second oscillation in Fig. 9 is much larger than the amplitude of the first oscillation. Based on what we argue below the third oscillation might have an even larger amplitude. This effect is not caused by defect structures, which only define the position of the minima in Fig. 9. The increase of amplitude is caused by the increase of the stacking fault probability which we found to be $P_{F,0}=11\%$, $P_{F,1}=33\%$, and $P_{F,2}=41\%$ for the substrate, first layer, and second layer. Assuming perfect layer-by-layer growth and absence of coalescence (and consequently self-healing) up to a layer coverage of 0.65 ML, this yields maxima values for θ_F of 7%, 21%, and 27%. The first two numbers are in decent agreement with experiment.

This rises the obvious question as to why P_F should be layer dependent. It is not remote to consider the possible effects of codeposited impurities. In homoepitaxy on Pt(111) it was proven that minute amounts of CO coadsorbed during evaporation give rise to drastic changes in the growth morphology.[30] In epitaxial growth of Co on Ru(0001) the nucleation probability for islands in two different stacking sequences was found to depend critically on the background pressure during deposition.[11] To test the possible influence of coadsorbed CO on stacking fault nucleation, 1.4 ML were deposited in an additional CO partial pressure of 4×10^{-4} mbar. No effect on $P_{SF,1}$ was found.

In distinction to the situation on the substrate, nucleation on the first or higher layers takes place in the presence of the step edges of trenches and holes not yet closed to the lower layer [compare Figs. 1(c) and 1(e)]. As adatoms are known to be trapped on the upper terrace at the step edge,[19] one could speculate that such adatoms or small clusters trapped at the step edge—trapped possibly even on stacking fault sites—could influence θ_F. To test this assumption the sample was first sputtered at 1000 K and about 0.3 ML was removed from the topmost layer. Under these temperature conditions the surface vacancies created due to sputtering nucleate on large terraces and form hexagonal vacancy islands while they anneal to descending step edges on terraces with a width below about 100 nm [compare Fig. 10(a)]. After sputtering 0.6 ML Ir was deposited at 350 K. On the large terraces the vacancy islands were almost filled and subsequently nucleation of adatom islands took place in the presence of step edges. In these areas we found $P_F=0.17$. On the narrow terraces for the evaluation of P_F we analyzed only islands not attached to step edges and find $P_F=0.10$ [compare Fig. 10(b)]. Although, due to the different growth situation the enhancement effect is not as strong as in pure homoepitaxy, this test experiment shows the decisive influence of step edges on the nucleation of stacking fault islands.

We consider trapping of adatoms or small clusters at step edges in stacking fault sites to be a likely origin of the enhancement effect. This assertion is consistent with the explanation for Ir adatoms and dimers to populate preferentially faulted sites.[31] For transition metals with increasing *d*-band filling a change from hcp to fcc stacking takes place. Ir has just a sufficient filling to obtain fcc stacking. Small cluster at the surface, however, experience through their reduced coordination a smaller effective *d*-electron density and thus are preferentially on hcp sites. Adatoms and dimers at step edges would experience an even lower effective *d*-electron density and could populate hcp sites with an even stronger preference. Step related surface strain was also postulated to influence P_F distant from steps in homoepitaxy on Cu(111).[32] To pinpoint the step related enhancement effect additional dedicated experiments are necessary.

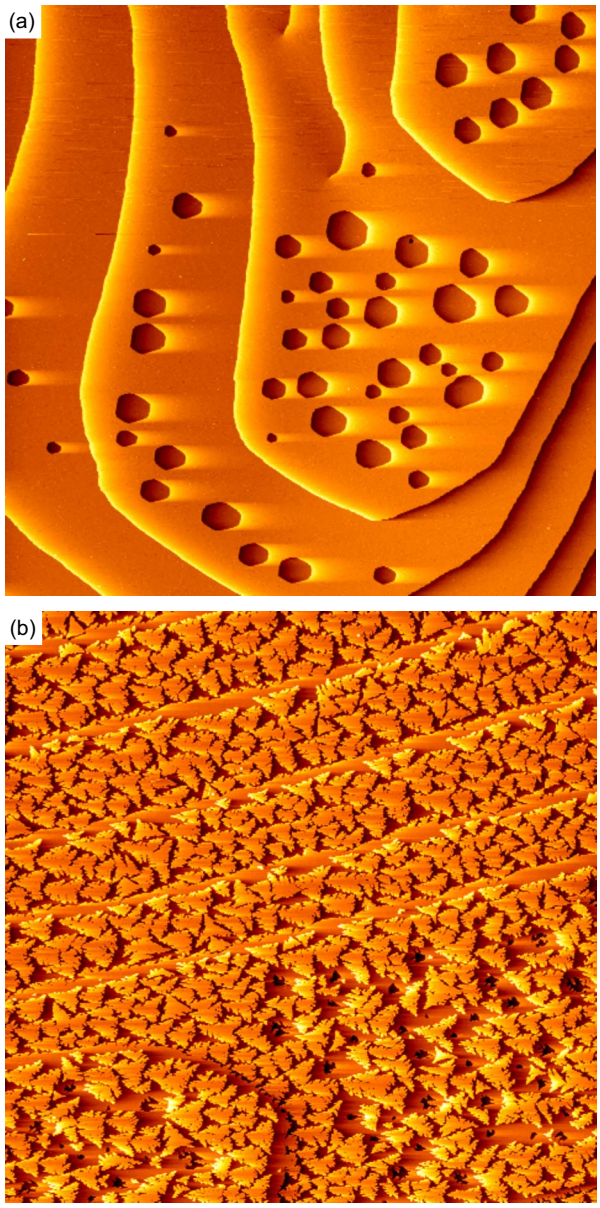

FIG. 10. (Color online) (a) Ir(111) after sputtering at 1000 K. (b) Topograph after additional deposition of 0.65 ML Ir at 350 K on the surface prepared in (a). See text. Image size is 540 nm $\times$ 540 nm.

While the enhanced P_F in higher layers increases the maxima in θ_F, this effect alone is not what eventually causes the majority of the surface to become twinned. This transformation is brought about by the processes increasing the level of the minima in θ_F and damping out the oscillations. Stack-

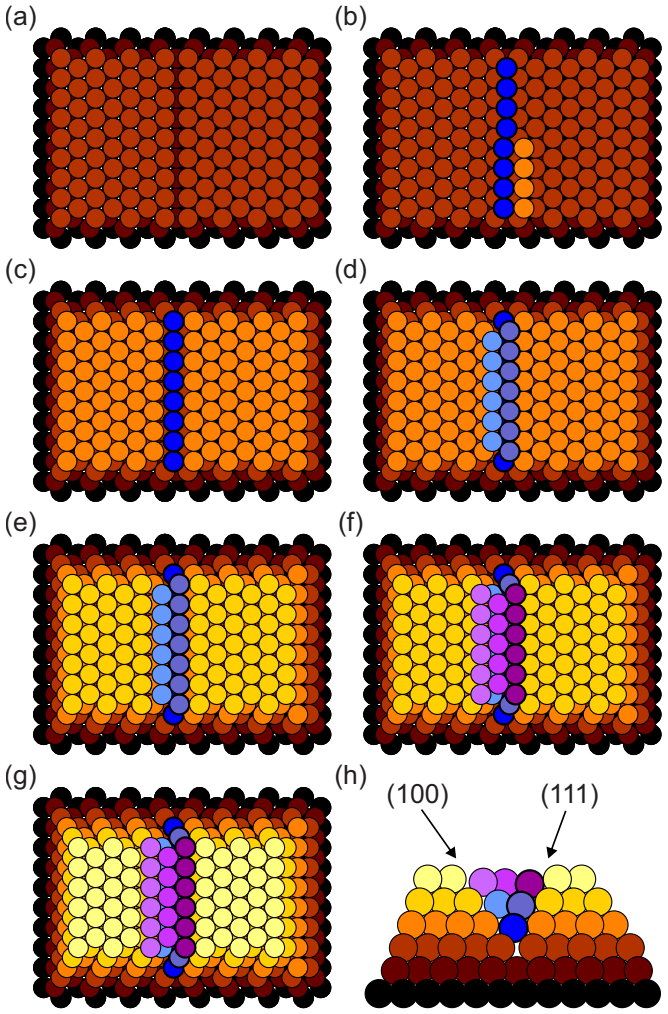

FIG. 11. (Color online) (a)-(g) Top view ball model cartoons on growth after introduction of a stacking fault on the left-hand side in (a). (h) Cross section through (g). See text.

ing fault areas are protected against self-healing through decoration row formation and form twin crystallite seeds. Once decoration rows are formed, they induce in higher layers stacking faults in the surrounding of the initial fault area and stabilize the new stacking sequence resulting in stable twins. As such twin seeds may be formed in each new layer, the amount of twinned surface area increases. As during growth the surface roughens and nucleation is eventually almost exclusively at defects and defect structures preserving the stacking sequence; oscillations die out and the majority of the surface transforms to the twinned state.

The ball model cartoons of Fig. 11 sketch the evolution of a twin crystallite and illustrate the general statements above. Upon close encounter a faulted area to the left of Fig. 11(a) (stacking sequence aba) forms an *A* gap with an unfaulted area (stacking sequence abc) on the right. The *A* gap becomes decorated through a thin decoration row in Fig. 11(b). Through the energetic avoidance of intrinsic stacking faults[14] (two faults in subsequent layers) atoms attaching to the decoration row will shift the decoration row atoms slightly to the left, thereby creating new fourfold coordinated adsorption sites. Further attachment under the constraint of optimum coordination of the attaching atoms results in the formation of an fcc twin crystallite (stacking sequence abac) on the left and the introduction of a new fault on the right (stacking sequence abcb) [compare Fig. 11(c)]. This introduction of the new fault to the right enlarges θ_F and is the key process for proliferation of twins. Note that a small gap remains to the left of the fourfold coordinated adsorption sites in Fig. 11(c). In the fifth layer again first the strongly bonding fourfold coordinated adsorption sites are filled [compare Fig. 11(d)]. Next, atoms cover the small gap formed by undercoordinated atoms right to the fourfold adsorption sites. After these two rows of atoms are adsorbed, forming a fat decoration row, further addition of atoms under the constraint of optimum coordination of the attaching atoms results in preserved stacking sequence on both sides of the defect structure: on the left the stacking sequence is abacb and on the right it is abcba [compare Fig. 11(e)]. Note that left to the fourfold coordinated adsorption sites a small gap in the layer remains. In the sixth layer again the fourfold coordinated adsorption sites are filled first and then the two rows left of them next to cover the small gap in the layer below. Now a three atom wide fat decoration row is formed [compare Fig. 11(f)]. Filling the sixth layer again under the constraint of optimum coordination of the attaching atoms results in the situation depicted in Fig. 11(g). No new stacking faults are introduced and the stacking sequences are abacba to the left and abcbac to the right. Note that during the sequence of cartoons in Figs. 11(a)–11(g) the fourfold coordinated adsorption sides move to the right while the gap moved to the left, creating an expanding defective area in between. The cross section in Fig. 11(h) shows that the defective area between the two twins is bounded by a (100) plane to the left and a (111) plane to the right. The central defective area has a lower atomic density (in each layer 1/3 of an atom row is missing) and is depressed. Continued growth will preserve the stacking sequence and extend the defective area which is initially bounded by (111) and (100) planes between the two twin crystallites.[33] Thus the twinned surface area will remain twinned during growth.

Based on our description, one might expect the entire surface to transform to the twinned state. At least up to 90 ML this is not the case. Our STM investigations do not allow to obtain a clue on the nature of incoherent twin boundaries separating a twinned crystal from an untwinned crystal, which could explain why not the entire surface becomes twinned. In thick films, adjacent to elongated mounds resulting from decoration row defect structures we frequently see deep grooves which could be such boundaries.

VI. SUMMARY

Using STM and LEED methods to determine the stacking fault covered surface area, it was possible to describe the evolution of this quantity with the deposited amount. We found that during initial layer-by-layer growth this quantity oscillates with an increasing amplitude due to the interplay of self-healing and a step-influenced probability of fault nucleation. Small patches of stacking fault area resisting self-healing through stabilizing decoration rows are the seeds for

twin crystallite formation. Such seeds cause twin crystallite formation in subsequent layers in their surrounding (proliferation). As more and more seeds and twin crystallites are formed, layer-by-layer growth is lost and rough growth takes place, which is dominated by heterogeneous nucleation at defect structures separating areas of differing stacking sequence.

ACKNOWLEDGMENTS

Support by the Deutsche Forschungsgemeinschaft through the project "Kinetics of stacking faults in thin films" and the critical reading of the manuscript by Carsten Busse is acknowledged.

*Corresponding author: bleikamp@ph2.uni-koeln.de

†Present address. Fachbereich Physik, Universit ät Konstanz, 78457 Konstanz, Germany

‡Present address. Dept. Física de la Materia Condensada, Universidad Autónoma de Madrid, 28049 Madrid, Spain

[1] T. Shinohara, T. Sato, and T. Taniyama, Phys. Rev. Lett. **91**, 197201 (2003).

[2] B. Sampedro, P. Crespo, A. Hernando, R. Litrán, J. C. Sánchez López, C. López Cartes, A. Fernandez, J. Ramírez, J. González Calbet, and M. Vallet, Phys. Rev. Lett. **91**, 237203 (2003).

[3] S. S. Alexandre, E. Anglada, J. M. Soler, and F. Yndurain, Phys. Rev. B **74**, 054405 (2006).

[4] F. Aguilera-Granja, J. M. Montejano-Carrizales, and A. Vega, Solid State Commun. **133**, 573 (2005).

[5] U. Lindefelt, H. Iwata, S. Oberg, and P. R. Briddon, Phys. Rev. B **67**, 155204 (2003).

[6] S. Ha, M. Skowronski, J. J. Sumakeris, M. J. Paisley, and M. K. Das, Phys. Rev. Lett. **92**, 175504 (2004).

[7] J. Wang, M. Tian, T. E. Mallouk, and M. H. W. Chan, J. Phys. Chem. B **108**, 841 (2004).

[8] M. Pratzer and H. J. Elmers, Phys. Rev. B **72**, 035460 (2005).

[9] W. L. Ling, N. C. Bartelt, K. F. McCarty, and C. B. Carter, Phys. Rev. Lett. **95**, 166105 (2005).

[10] F. E. Gabaly, W. L. Ling, K. F. McCarty, and J. de la Figuera, Science **308**, 1303 (2005).

[11] F. E. Gabaly, J. M. Puerta, C. Klein, A. Saa, A. K. Schmid, K. F. McCarty, J. I. Cerda, and J. del la Figuera, New J. Phys. **9**, 80 (2007).

[12] C. Polop, I. Mora-Seró, C. Munuera, J. G. de Andrés, V. Munoz-Sanjosé, and C. Ocal, Acta Mater. **54**, 4285 (2006).

[13] P. Zoontjens, T. P. Schulze, and S. C. Hendy, Phys. Rev. B **76**, 245418 (2007).

[14] S. Bleikamp, A. Thoma, C. Polop, G. Pirug, U. Linke, and T. Michely, Phys. Rev. Lett. **96**, 115503 (2006).

[15] T. Michely, M. Kaiser, and M. J. Rost, Rev. Sci. Instrum. **71**, 4461 (2000).

[16] I. Horcas, R. Fernandez, J. M. Gomez-Rodriguez, J. Colchero, J. Gomez-Herrero, and A. M. Baro, Rev. Sci. Instrum. **78**, 013705 (2007).

[17] T. Michely and J. Krug, *Islands, Mounds and Atoms*, Springer Series in Surface Sciences Vol. 42 (Springer-Verlag, Berlin, 2004).

[18] A. Thoma and T. Michely (unpublished).

[19] S. C. Wang and G. Ehrlich, Phys. Rev. Lett. **67**, 2509 (1991).

[20] M. Müller, K. Albe, C. Busse, A. Thoma, and T. Michely, Phys. Rev. B **71**, 075407 (2005).

[21] C. Busse, C. Polop, M. Müller, K. Albe, U. Linke, and T. Michely, Phys. Rev. Lett. **91**, 056103 (2003).

[22] C. Busse and T. Michely, Surf. Sci. **552**, 281 (2004).

[23] M. J. Stowell, *Epitaxial Growth*, edited by J. W. Matthews (Academic, New York, 1975), Pt. B, Chap. 5, p. 437.

[24] J. C. Hamilton, M. R. Sorensen, and A. F. Voter, Phys. Rev. B **61**, R5125 (2000).

[25] C. Polop, A. Lammerschop, C. Busse, and T. Michely, Phys. Rev. B **71**, 125423 (2005).

[26] J. B. Pendry, *Low Energy Electron Diffraction* (Academic, London, 1974).

[27] M. A. van Hove, W. H. Weinberg, and C. M. Chan, *Low-Energy Electron Diffraction* (Springer-Verlag, Berlin, 1986).

[28] K. Meinel, M. Klaua, and H. Bethge, Phys. Status Solidi A **110**, 189 (1988).

[29] S. Bleikamp, J. Coraux, and T. Michely (unpublished).

[30] M. Kalff, G. Comsa, and T. Michely, Phys. Rev. Lett. **81**, 1255 (1998).

[31] S. Papadia, B. Piveteau, D. Spanjaard, and M. C. Desjonqueres, Phys. Rev. B **54**, 14720 (1996).

[32] M. Giesen and H. Ibach, Surf. Sci. **529**, 135 (2003).

[33] While it is likely that the (111) plane defined by the locations of the fourfold coordinated adsorption sites remains a boundary of one twin crystallite, this is not obvious for the other twin crystallite boundary starting out as a (100) plane. From the STM topographs it appears that the width of the defective area between the two crystallites stays limited to several nanometer even for the thickest deposited films. Thus, the initial (100) facet probably does not stay in this orientation for thicker films.